# Robust Damping and Decoupling Controller for Interconnected Power Network based on Distributed Energy Resources

Mohamed Ahmed[a]1, F. Alsokhiry[b], Khaled H. Ahmed[c], Ayman Samy Abdel-Khalik[d], Y. Al-Turki[b]

[a] *Department of Engineering Mathematics and Physics, Alexandria University, Alexandria 21544, Egypt*
[b] *Department of Electrical Engineering, King Abdulaziz University, Jeddah 21589, Saudi Arabia*
[c] *Department of Electronic and Electrical Engineering, Strathclyde University, Glasgow, G1 1XQ, UK*
[d] *Department of Electrical Engineering, Alexandria University, Alexandria 21544, Egypt*

**Abstract**

Converter based distributed energy resource (DER) units are intended to be integrated into the power system using grid-forming converters (GFCs). It proposes to emulate the synchronous machines dynamics and forms the grid voltage/frequency by instantaneously balance the load changes without peer-to-peer coordination. However, the damping and coupling characteristics of GFCs in multi-vendor interoperability-based network have not yet been fully explored. The paper proposes a step-by-step analytic method based on participation factor analysis to efficiently analyze the oscillatory modes and the coupling characteristics in the GFCs-based network, especially where the GFCs are controlled by different control techniques. Moreover, to efficiently damp these oscillatory modes and such control coupling, a hybrid damping method based on an oscillation damper and a decoupling controller is proposed. A mathematical modelling is derived to confirm the role of the proposed decoupling controller especially during transient periods. Design guidelines using pattern search algorithm are presented to identify the optimum parameters of the proposed hybrid damping method. Finally, the experimental results using Controller-hardware-in-the-loop (CHiL) verify the theoretical analysis and the efficient damping against large disturbances.

*Keywords:* Grid-forming converters, converter dominated network, weak grid, decoupling controller, pattern search.

## 1. Introduction

Grid-forming converter represents an emerging technology that allows renewable energy generation integration into conventional power network. However, as the renewable generators penetration increases, the injected power share based on synchronous generators drops, which reduces the overall system inertia and leads to significant consequences on the power system stability [1]. Therefore, various control methods for GFCs have been proposed in literature to support the network frequency and voltage at the point of common coupling (PCC) and high inertia are the essential features for maintaining a stable power. Among of these control methods, $P-f$ or $Q-v$ droop control is the simplest and common technique [2, 3]. Droop control mimics the function of governor and exciter in synchronous generators, which instantaneously balances loads based on frequency and voltage deviations without a dedicated communication architecture. An alternative control method for GFCs is the virtual synchronous generator (VSG) [4, 5], which emulates the basic features of synchronous generators by providing a virtual inertia and damping through the swing equation. However, this equation requires an information about the converter active power, that may not be accessible in some applications [6]. Another control method for GFCs is the DC-matching, which solves the issue of the converter active power inaccessibility. The DC-matching method provides the required inertia and damping by controlling the converter dc-link dynamics [7, 8]. These previously stated control methods (Droop, VSG, and DC-matching) can be fitted with phase-locked loop (PLL) to improve the deduction of the synchronization angle with the network whose its effects on stability have been highlighted in [9, 10]. In multi-vendor interoperability-based network, the GFCs are connected together; where each GFC may has a unique control method that differs from the other GFCs. However, there is no study in literature to analyze and efficiently damp the oscillations in GFCs-based network, where different control methods are used.

This is a peer-reviewed, accepted author manuscript of the following article: Ahmed, M., Alsokhiry, F., Ahmed, K. H., Abdel-Khalik, A., & Al-Turki, Y. (2023). Robust damping and decoupling controller for interconnected power network based on distributed energy resources. International Journal of Electrical Power & Energy Systems, 145, [108581]. https://doi.org/10.1016/j.ijepes.2022.108581

One key observation is that, regardless of the method the GFC is controlled, the GFC control structure includes two main loops, namely, $P-f$ (active power loop) and $Q-v$ (reactive power loop). Moreover, one of the most proper features of the GFC control is its damping characteristics against network disturbances. The damping effect may be implemented in the $P-f$ loop or the $Q-v$ loop. For instance, the damping in the $P-f$ control loop is addressed by any of the following methods: (i) The damping that is realized based on the difference between the virtual speed (estimated by the swing equation or the dc matching loop) and the nominal speed as in [11]. However, this method deteriorates the inertial response as it introduces an offset if the speed is not properly estimated. (ii) The method introduced in [12, 13] mimics the damping based on the derivative of the speed or the active power, respectively, to avoid the steady state error in the speed estimation. However, it requires a proper filter design for the derivative action to provide a strong damping without deteriorating the inertial response. (iii) The method in [14] has introduced the required damping through the difference between the nominal and measured (not estimated) speeds. But it relies on a PLL that cannot properly operate in case of weak grids. On the other hand, the required damping can be achieved in the $Q-v$ control loop. The idea was inspired from the power system stabilizer (PSS) in synchronous generators. PSS applies the damping in form of voltage magnitude ($v_{damp}$), which is added to the output of the AVR control block. For instance, authors in [15] had applied the damping in the $Q-v$ loop through a low path filter and a derivative action. However, this approach does not give adequate damping against certain types of disturbances that include swing changes.

Another key observation is that the damping improvement can be indirectly achieved by improving the decoupling characteristics of the GFC. Moreover, the idea of controlling the GFC including two simple separate loops, $P-f$ and $Q-v$ is efficient when the active and reactive power components are decoupled. This theoretical decoupling is hard to be developed in most of grid conditions ($R/X$ ratio) and during transients [16]. the authors in [17] reduces the cross coupling in the GFC control using compensating terms, however, these terms were highly dependent on the estimated speed, which is generally inaccurate during transient conditions. In [18] and [19], the coupling effect was addressed using a virtual impedance and virtual negative resistor, respectively. These components should properly be designed as they have a negative impact on the inertial responses and damping characteristics. In [12], the GFC control was augmented with a damping correction loop leading to a lower coupling between the power components. However, this approach slows down the response speed. The approach in [16] has combined the damping correction loop with a transient droop function to reduce the coupling and improve the GFC response speed, however, at the cost of added complexity and heavy computational burden.

From the discussion above, it can be concluded that there are shortcomings in the GFC control methods. First, the damping characteristics are analysed and designed for only local oscillations of one standalone/grid-tied converter without any consideration to the oscillations occurred in interconnected power system based on distributed energy resources, where the GFCs are interconnected and controlled by different control methods. Second, there is no decoupling controller that has been developed so far to simply compensate between the direct and quadrature axes during transient without compromising on the level of control complexity, speed response, and implementation simplicity. Third, the problem of multi reference frames for GFCs is not addressed as the converters in ac systems are usually modelled in a rotating reference frame aligned to a local measurement angle. Therefore, to model the whole system, these are firstly locally referenced then they have to be aligned (rotationally transformed) to a global reference frame. This problem needs to be fully explored, since most existing literature aims to model the GFC in the local reference frame.

In the synchronous machine-based network, there is an oscillatory relationship (mode) between the synchronous machine and a power system, and between synchronous machines in the power system. These oscillation modes and their effects on power system stability are discussed for the synchronous machine-based network in [20]. However, identifying the dominant oscillatory modes in a converter-based power network with low or no inertia have not yet been fully explored. This paper investigates the dominant oscillatory modes that are raised in GFCs-based power networks. The study reveals that, along with the frequency dependent decoupling terms, excessive transient spikes can transfer between the control loops or even cause instability, especially during the transient periods or until the synchronization takes place. In addition, the coupling between converter control loops has a direct impact on the system oscillatory modes and stability. To efficiently damp these oscillatory modes and such control coupling, a hybrid damping method based on an oscillation damper and a decoupling controller is proposed. A mathematical modelling is derived to confirm the role of the proposed decoupling controller especially during transient periods. Moreover, the mathematical model is extended to tackle the key challenges related to integrative modelling of GFCs-based power network such as multiple reference frames and interoperability under different control techniques. The proposed hybrid damping method design procedures are discussed to identify the control parameters. The proposed design procedures are distinctive as follows: (i) analysing the oscillatory modes in the integrative model according to their severity using the participation factor analysis, (ii) optimally identifying the proposed control parameters based on the pattern search

algorithm to efficiently damp these severe oscillations especially the inter-area oscillations, (iii) considering the multi-operational conditions as in the case of power system planning using economical dispatch, (iv) conserving the synchronization stability against different types of large disturbances. The key paper contributions are summarized as follows:

- Identifying and characterizing the dominant oscillatory modes, which arise as a result of interaction between GFCs in a converter-based power network, which have not been investigated before.
- Deriving mathematical modelling to tackle the challenges related to the integrative model of GFCs-based power network such as multiple reference frames and interoperability under different control techniques.
- Proposing a hybrid damping method through an oscillation damper and a new decoupling controller for interconnected GFCs-based power network under different control techniques.
- Developing design guidelines (based on the pattern search algorithm and participation factor analysis) to optimally identity the parameters of the proposed hybrid damping method.

This paper is organized as follows; Section II presents an overview of the network structure. The whole non-linear state-space model is derived in Section III. Section IV describes the linearization of the state-space model. Section V covers the proposed hybrid damping method including the damper and decoupling controllers. Section VI covers the optimal design of control parameters using pattern search algorithm. Results are presented in Section VII using CHiL via OPAL-RT real time simulator and digital signal processor (DSP).

## 2. OVERVIEW OF THE SYSTEM STRUCTURE

This section discusses the network structure employed in the study and reviews the conventional GFC's control techniques, which will be modified in the following sections to improve the damping and decoupling characteristics. The ring distribution system of IEEE 9 bus test system, shown in Fig. 1, is selected for the study. However, the proposed control concept can still be extended to any number of buses. The test network consists of 3 converters operating in the grid forming mode with different control methods and are connected to buses 1, 2 and bus 3 through LCL filters. The loads are placed at buses 3, 4 and 5, respectively. The GFC buses and load buses are interconnected through 100 km distribution lines with an impedance $\boldsymbol{Z_{Dl}}$. The GFC operates as a controllable voltage source, whose output power is determined by the network conditions. The control strategies for GFCs assume a weak network with uncertain voltage/frequency during the disturbance and the main role of such controllers is to support and preserve the network voltage/frequency by suppling the network with required power in a manner similar to synchronous generators. The conventional control technique for the GFC is shown in Fig. 2. The resistors $\boldsymbol{R_1}$ and $\boldsymbol{R_2}$ represent the resistances of the filter inductor, while $\boldsymbol{R_d}$ is placed in series with the capacitor and has a major role for damping the resonant frequency of the LCL filter. The converter is controlled using the droop control method, which curtail the need for a dedicated communication system between the different converters in interconnected systems. The output of the inverter is passed through an LCL filter to reject the high-frequency switching noise. The filtered voltage and current measurements are then transformed to $\boldsymbol{dq}$-axis components using a reference frame transformation. The converter's instantaneous power components $(\boldsymbol{p}, \boldsymbol{q})$ is calculated based on these measurements. The calculated powers are filtered out to remove high switching noise due to measurements, then the filtered power components $(\boldsymbol{P}, \boldsymbol{Q})$ are sent to the droop controller. Droop controllers set voltage and frequency references based on the current level of active and reactive power being generated. These voltage and frequency references are then compared with the measured voltage and frequency. The error signal obtained by comparing the reference values and measured values are passed through the voltage PI controllers to generate references for the current flowing through the output filter inductor. These reference current signals are then compared with the corresponding measured filter inductor currents and are passed through another current PI controllers to generate the voltage that should be appeared at the converter terminals. As mentioned before, an accurate frequency measurement is needed for the PI voltage controllers to operate. One key issue of GFC is that it is assigned to interact with a non-stiff grid with uncertain frequency. Therefore, precise frequency measurement is challenging. This issue is remedied by synchronization unit, whereas the frequency may be accurately measured by the synchronization unit in two primary ways; (i) similar to synchronous machines which balances the energies to reach frequency consensus as in virtual synchronous machine (VSM), and DC matching control, (ii) forcing the d-axis component of the voltage to zero in a $\boldsymbol{dq}$-based PLL. This synchronization unit not only measures the frequency of the system but also calculates the phase angle of the voltage. This angle is used to make all the conversions between stationary and synchronous reference frames. All controllers are modeled in the individual reference frame local to each inverter as determined by the phase angle from the synchronization unit. To validate the condition of multi-vendor interoperability, each GFC will use a synchronization technique differs from the other GFCs. Therefore, the synchronization unit in Fig. 2 contains the three common synchronization techniques in literature

(VSM, PLL, DC matching), and each GFC from the three converters uses different synchronization technique. The power converter dynamics are affected by the controller and network parameters, therefore, a nonlinear state space model for the overall system is derived to control these dynamics and study the multi-reference frames.

## 3. NONLINEAR STATE SPACE MODELING

This section discusses the dynamic equations and the nonlinear state space model of the proposed network shown in Fig. 1. Subsequently, the controller parameters are optimally designed in the integrative model.

### *3.1. Droop controller*

In grid-connected mode, the magnitude of the grid voltage determines the inverter's output voltage. The PLL ensures accurate tracking of grid phase to keep inverter output synchronized with the grid. During operation in islanded mode or with a non-stiff grid, the inverter lacks these externally supplied reference signals by the grid. The droop equations must therefore be used to enable the inverter to generate its own frequency and voltage magnitude references.

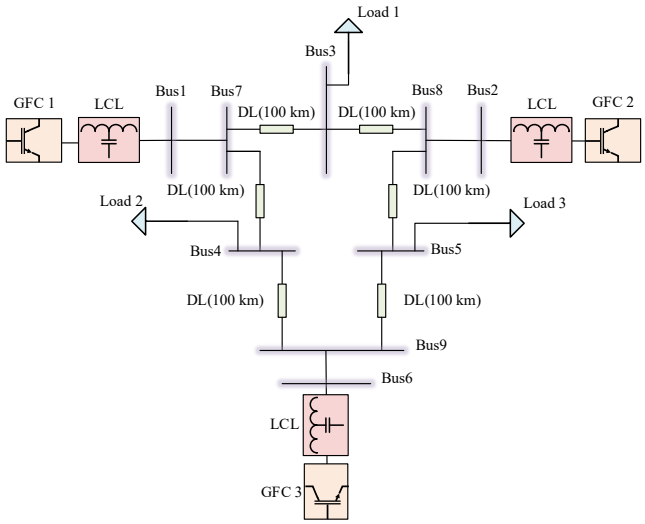


Fig. 1. The proposed network test system.

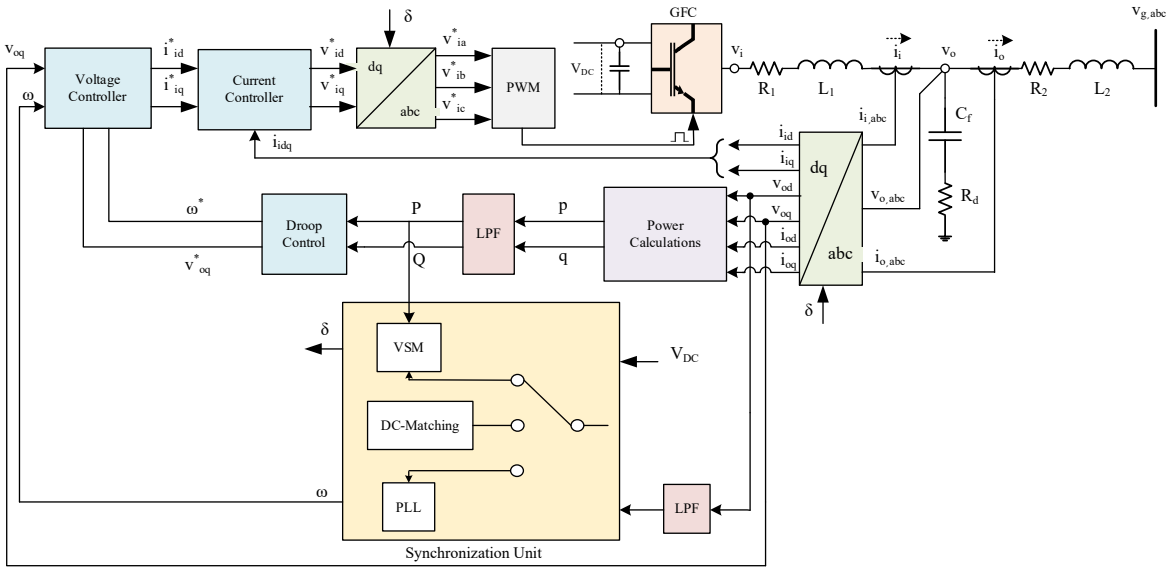


Fig. 2. The control structure for the GFC.

The droop controller consists of two-line equations with negative slops. These equations generate the reference voltage magnitude and frequency based on the value of the converter active and reactive power components, as shown in (1) and (2).

$$\omega^* = \omega_n - mP \quad (1)$$

$$v_{oq}^* = v_{oq,n} - nQ \quad (2)$$

where $\omega_n$ and $v_{oq,n}$ are the nominal frequency and voltage respectively, $P$ and $Q$ represent the filtered active and reactive power for the power converter, $m$ and $n$ are the droop constants, which control the power sharing between GFCs.

*3.2. Converter power calculations*

The average power components are required for the droop equations and synchronization unit. Therefore, the instantaneous output active $p$ and reactive power $q$ are calculated from the dq components of the output voltages and currents. Then, the filtered power components $(P, Q)$ are calculated by passing the instantaneous components through a low-pass filter, as shown in the following equations,

$$P = \frac{\omega_c}{s+\omega_c} p\,, \quad Q = \frac{\omega_c}{s+\omega_c} q \quad (3)$$

$$P' = -P\omega_c + \omega_c\left[1.5\left(v_{od} i_{od} + v_{oq} i_{oq}\right)\right] \quad (4)$$

$$Q' = -Q\omega_c + \omega_c\left[1.5\left(v_{od} i_{oq} - v_{oq} i_{od}\right)\right] \quad (5)$$

where $v_{od}, v_{oq}$ are the output voltage across the LCL filter and $i_{od}, i_{oq}$ are the output current in the dq reference frame, $\omega_c$ is the cutoff frequency of the low-pass filter.

*3.3. Synchronization unit*

This unit is responsible for estimating (measuring) the actual angular speed of the system, then determining the synchronization angle required for all Park's transformations. For simplicity, this unit is implemented to include only the most three common techniques, namely, PLL, VSM, or dc-matching, as previously explained. However, this unit can be extended to include other techniques in literature. Each GFC in test network uses only one of those technique (through a three-position switch) as shown in Fig. 2. Consequently, each GFC uses different synchronization technique to test and validate system interoperability condition.

*A) PLL*

This technique locks its output with the network phase voltage to estimate the system frequency. In this paper, the phase is locked such that $\boldsymbol{v_{od} = 0}$. Equations are described as follows:

$$v'_{od,f} = (v_{od} - v_{od,f})\omega_{c,PLL} \quad (6)$$

$$\vartheta' = v_{od,f} \quad (7)$$

$$\omega = \omega_n - K_{p,PLL} v_{od,f} - K_{i,PLL}\vartheta, \quad \delta' = \omega \quad (8)$$

where, $v_{od,f}$ is the filtered $d$ component of the output voltage across the filter capacitor, $\omega_{c,PLL}$ is the cutoff frequency of the PLL low pass filter, $K_{p,PLL}, K_{i,PLL}$ are the gains for the PLL PI controller, and $\omega, \delta$ are the estimated angular frequency and synchronization angle, respectively.

*B) VSM*

This technique depends on the virtual swing equation to estimate the system frequency, as follows:

$$\omega' = \Delta P/\omega_n J \quad , \quad \Delta P = P_n - P - P_{Damp} \tag{9}$$

$$P_{Damp} = D_{damp}(\omega_n - \omega) \tag{10}$$

where, $P_n$ is the nominal active power for the GFC, $J$ is the virtual moment of inertia, $D_{damp}$ is the damping factor and $P_{Damp}$ is the damping power.

*C) DC-MATCHING*

This technique depends on the duality between the virtual electro-mechanically (swing equation) and electrically (dc bus) models to estimate the system frequency. Therefore, dc-link current is used as an equivalent to the power converter active power, while dc-link capacitance is equivalent to the moment of inertia, as shown in [21] and described as follows:

$$V'_{dc} = \Delta I/C_{dc}, \qquad \Delta I = I_s - I_{dc} - I_{damp} \tag{11}$$

$$I_{Damp} = YV_{dc}, \ \omega \equiv V_{dc}/\ k_{tr} \tag{12}$$

where $I_s$ and $I_{dc}$ are the input and output currents of the dc-link, respectively. $C_{dc}, Y$ is the capacitance and admittance for the dc-link, respectively. $I_{Damp}$ is the damping current and $k_{tr}$ is the compensation gain between angular speed and dc voltage.

*3.4. Voltage and current controllers*

The voltage and current controllers regulate the output capacitor voltage and output inductor current.

*A) Voltage controller*

The reference frequency ($\boldsymbol{\omega}^*$) and reference q axis voltage ($\boldsymbol{v}^*_{\boldsymbol{oq}}$) from the droop control are compared with the estimated frequency from the synchronization unit ($\boldsymbol{\omega}$) and the measured q axis voltage ($\boldsymbol{v}_{\boldsymbol{oq}}$), respectively. Then, the error signals are used to generate the reference d and q axis current components ($\boldsymbol{i}^*_{\boldsymbol{id}}, \boldsymbol{i}^*_{\boldsymbol{iq}}$) for the cascaded PI current controllers, as follows.

$$\emptyset'_{v,d} = \omega - \omega^* \tag{13}$$

$$i^*_{id} = k_{i,vd}\emptyset_{v,d} + k_{p,vd}\emptyset'_{v,d} \tag{14}$$

$$\emptyset'_{v,q} = v^*_{oq} - v_{oq} \tag{15}$$

$$i^*_{iq} = k_{i,vq}\emptyset_{v,q} + k_{p,vq}\emptyset'_{v,q} \tag{16}$$

where, ($k_{i,vd}, k_{p,vd}$) and ($k_{i,vq}, k_{p,vq}$) are the voltage PI controller's gains for direct and quadrature axis, respectively.

*B) Current controller*

The reference $dq$ current components ($i^*_{od}, i^*_{oq}$) are compared with the measured output inductor current($i_{od}, i_{oq}$). Then, the error signals generate the reference $dq$ voltage components ($v^*_{id}, v^*_{iq}$) using two PI controllers. The cross-coupling between the d-axis and q-axis is eliminated, as follows;

$$\emptyset'_{i,d} = i^*_{od} - i_{od} \tag{17}$$

$$v^*_{id} = k_{i,cd}\emptyset_{i,d} + k_{p,id}\emptyset'_{i,d} \underbrace{-\omega_n L_1 i_{oq}}_{cross-coupling} \tag{18}$$

$$\emptyset'_{i,q} = i^*_{oq} - i_{oq} \tag{19}$$

$$v^*_{iq} = k_{i,cq}\emptyset_{i,q} + k_{p,iq}\emptyset'_{i,q} \underbrace{+\omega_n L_1 i_{od}}_{cross-coupling} \tag{20}$$

where, $(k_{i,cd}, k_{p,id})$ and $(k_{i,cq}, k_{p,iq})$ are the current PI controller's gains. It is worth mentioning that the cross-coupling elimination is not efficient during the transient as it depends on $\omega_n$, which is improper during the transient. This problem is addressed rigorously by the proposed hybrid damping method.

### *3.5. LCL filter*

The modulating voltage signals generated from the current controller are passed to the PWM to generate the corresponding switching signals. For simplicity, the power converter losses as well as the forward voltage of the semiconductor switches are neglected. Hence, $\boldsymbol{v^*_{i,abc} = v_{i,abc}}$. The output converter voltages are filtered through an LCL filter. The 6 state equations for the LCL filter are described in [22].

### *3.6. Loads and distribution line*

In this study, loads are modelled as inductive, which represents many practical loads. For simplicity and to reduce the number of states, the short lines model of transmission lines is considered in this study and modelled as a series lumped resistance and inductance which ignoring the shunt capacitance. However, incorporating shunt capacitance will not provide a significant challenge, since the equations will be similar to those of an LCL filter as described in [23].

### *3.7. The global and local reference frames*

A major question that arises when modelling and analysing the interconnected power systems in the $\boldsymbol{dq}$ frame is how power converters that rotate with different speeds will be linked together or how the reference frame is chosen. Commonly for synchronous machines-based networks, the network is modelled in the $\boldsymbol{dq}$ frame based on a unified global reference frame that rotates with a constant speed $\boldsymbol{\omega_n}$. This nominal speed can be chosen based on two approaches, (1) if the system is connected to an infinite bus, then $\boldsymbol{\omega_n}$ represents the frequency of the infinite bus, (2) if no generator has a sufficient large inertia to be modelled as an infinite bus, then $\boldsymbol{\omega_n}$ is selected to be the steady-state system speed, which is the case for this study. Therefore, under steady state, the system will rotate with a constant speed and constant $\boldsymbol{dq}$ components (dc). Even though, the GFCs have a constant speed at steady state, their synchronization angles δ differ between them as each converter measures its synchronization angle according to its local frame. The employed modelling strategy in this paper divides the entire system into three primary submodules: converter, network, and loads. Each converter is modelled on its local reference frame whose rotation frequency is set by its synchronization unit. The converter model includes the controller dynamics, output filter dynamics, coupling inductor dynamics and voltage and current controller dynamics. Network dynamics are generally neglected in small-signal modelling of conventional power systems. The reason behind this is that the time constants of the rotating machines and their controllers are much larger than those of the network. In the case of microgrids, the micro sources are connected through converters whose response times are very small and network dynamics would influence the system stability. Therefore, the individual converter state equations are derived in terms of their perspective local reference frame and a transformation is necessary to translate between values defined in the local reference frame to the global reference frame in order to model the network dynamics. This issue has not been investigated in the GFC's research literature. Although it is not considered as a big issue in the standalone mode, it is very important in GFCs-based network to accurately model the interconnected network. In this paper, the GFC 1 is chosen to serve as a global reference frame for the other two GFCs, and its phase angle $\boldsymbol{\delta_1}$ is set up as a reference for the entire system. This

process is described in Fig. 3(a), which shows the three GFCs, each converter has its Park's transformation, which is derived based on individual local reference frame. Theses transformations are then referred to the global frame using the local to global transformation block and vice-versa. Fig. 3(b) describes the local reference frame for GFC 1 $(d_1, q_1)$, which is chosen to be the global reference frame $(D, Q)$ and the two local $dq$ frames corresponding to GFC 2 $(d_2, q_2)$ and GFC 3 $(d_3, q_3)$. $\theta_k$ is the difference between the global reference frame and local reference frame for GFC $k$ and calculated as follows:

$$\theta_k = \delta_1 - \delta_k, \qquad \delta_1 = 0 \tag{21}$$

where, $k$ is the number of the GFCs.

Moreover, the transformation from the local $(dq)$ to global $(DQ)$ frames and vice versa can be described as follows:

$$\begin{bmatrix} v_{d_k} \\ v_{q_k} \end{bmatrix} = \begin{bmatrix} cos(\theta_k) & -sin(\theta_k) \\ sin(\theta_k) & cos(\theta_k) \end{bmatrix} \begin{bmatrix} v_{D_k} \\ v_{Q_k} \end{bmatrix} \tag{22}$$

$$\begin{bmatrix} i_{Dk} \\ i_{Q_k} \end{bmatrix} = \begin{bmatrix} cos(\theta_k) & sin(\theta_k) \\ -sin(\theta_k) & cos(\theta_k) \end{bmatrix} \begin{bmatrix} i_{d_k} \\ i_{q_k} \end{bmatrix} \tag{23}$$

*3.8. The buses voltage equations*

The buses voltages can be written and modelled in terms of the system states using the concept of virtual resistor [24], which is shown in Fig. 4, and described as follows:

$$v_{g(i),D} = R_v(i_{Line(i),D} + i_{o(i),D} - i_{Load(i),D}) \tag{24}$$

$$v_{g(i),Q} = R_v(i_{Line(i),Q} + i_{o(i),Q} - i_{Load(i),Q}) \tag{25}$$

where, $R_v$ is a virtual resistor with high resistance (100 times the largest resistance in the system), so, its impact on the system dynamics is minimal. The derived non-linear equations will be linearized to tune the controllers' parameters

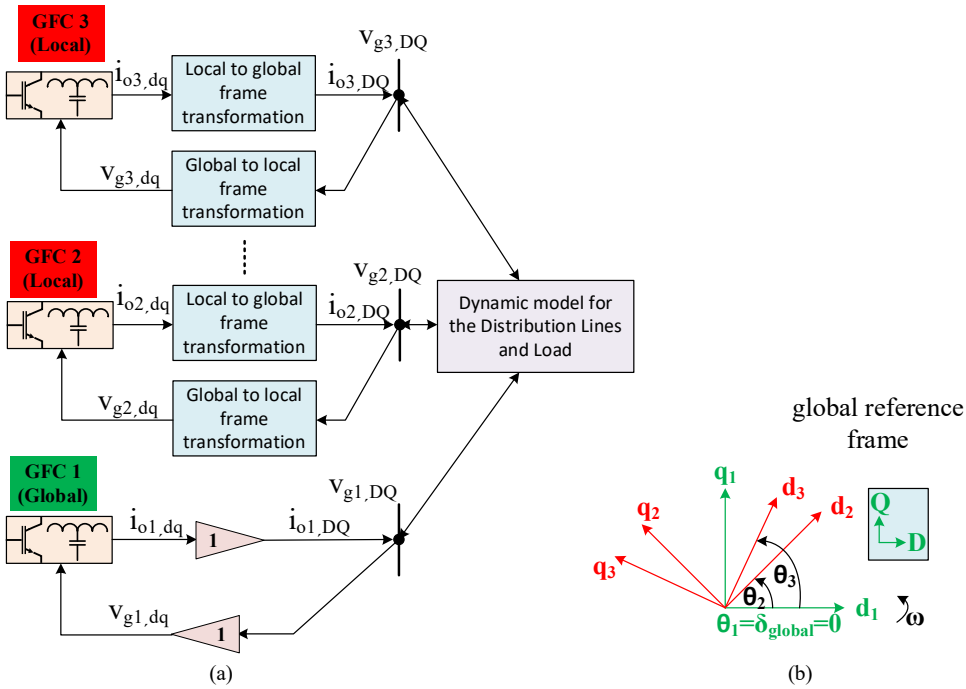


Fig. 3. The whole system modelling in the $dq$ frame for multi-reference frames, (a) Frame transformations, (b) Transformation angles.

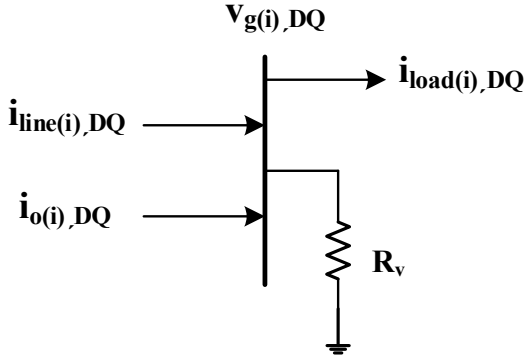


Fig. 4. The whole system model in the $\boldsymbol{dq}$ frame.

## 4. LINEARIZED STATE SPACE MODEL

The section discusses the linearization for the previously derived non-linear model to design the GFCs' hybrid damping methods properly. The dominated oscillatory modes of the system are investigated by model analysis, and participation factor analysis are described to reveal which states that are influencing these modes. The dynamic characteristics for the GFC dominated power network can be organized and described by a set of differential equations (states) given in (26). Moreover, the network and controller characteristics can be described using a set of non-linear algebraic equations given by (27).

$$x' = f(x, y) \tag{26}$$

$$0 = g(x, y) \tag{27}$$

where, $x$ and $y$ are the dynamic and algebraic state vectors, respectively. $f$ and $g$ are the set of differential and algebraic equations, respectively. Each power converter consists of 15 states in the PLL mode and 14 states in VSM/DC-matching modes. Each load consists of 2 states and each transmission line between 2 buses consists of 2 states, as follows;

$$x_{GFC\,k} = [P \quad Q \quad v_{od,f} \quad \emptyset \quad \delta \quad \emptyset_{v,d} \quad \emptyset_{v,q} \quad \emptyset_{i,d} \quad \emptyset_{i,q} \quad v_{od} \quad v_{oq} \quad i_{id} \quad i_{iq} \quad i_{od} \quad i_{oq}]_{\,k} \tag{28}$$

$$x_{line(ij)} = [i_{line(ij),D} \quad i_{line(ij),Q}] \tag{29}$$

$$x_{load(i)} = [i_{load(i),D} \quad i_{load(i),Q}] \tag{30}$$

The system is linearized using Jacobian linearization method [25]. The Jacobian approach uses the Taylor series expansion around an operating point $(x_0, y_0)$ as follows:

$$x' = f(x_0, y_0) + \frac{\partial f}{\partial x}\Delta x + \frac{\partial f}{\partial y}\Delta y + HOT \tag{31}$$

$$0 = g(x_0, y_0) + \frac{\partial g}{\partial x}\Delta x + \frac{\partial g}{\partial y}\Delta y + HOT \tag{32}$$

The higher-order terms (HOT) are ignored and the model equations $f(x_0, y_0)$, $g(x_0, y_0)$ are zero at the equilibrium operating point, and the equations are reformulated as follows:

$$x' = \frac{\partial f}{\partial x}\Delta x + \frac{\partial f}{\partial y}\Delta y = A\Delta x + B\Delta y \tag{33}$$

$$0 = \frac{\partial g}{\partial x}\Delta x + \frac{\partial g}{\partial y}\Delta y = C\Delta x + D\Delta y$$

Moreover, the vector related to algebraic state vector $(\Delta y)$ can be eliminated between the two sets of equations in (33) and the system state equations can be described as follows:

$$\Delta x' = (A - BD^{-1}C)\Delta x = A_{sys}\Delta x \tag{34}$$

where, $A_{sys}$ represents state matrix and describes the overall system dynamics. The equations are linearized using MATLABs symbolic math toolbox, which is provided as a supporting file. This linear model is used to linearize GFCs-based network around operating points and loading conditions.

## 5. THE PROPOSED HYBRID DAMPING METHOD.

This section proposes a hybrid damping method in the conventional GFC control technique to improve the damping characteristics mainly and address the cross-coupling issue between the control loops. This hybrid method consists of two basic parts (decoupling controller and damper) that will be added after the PI voltage controller.

### *A) Proposed decoupling controller*

The cross-coupling between the quadrature and direct loops (power components) can approximately be eliminated using the decoupled terms shown in (18) and (20), which depends on $\omega_n$. These decoupled terms work properly during the steady state operation because the estimated frequency for every GFC is equal to the nominal system frequency $\omega_n$. However, during disturbances, these frequencies will be different until synchronization takes place. This inefficient decoupling between loops causes critical issues to the power grid performance especially in the damping characteristics. For instance, during faults, the reactive power is increased significantly with transient spikes, and this reactive power response will be translated to the active power response if the coupling between loops is significant. Therefore, in the proposed controller, a compensating term is added to the direct voltage component ($v_{id}^*$) of the power converter output. This added term is linearly proportional to the quadrature voltage component ($v_{iq}^*$) using a gain ($K_1$), as shown in Fig. 5, which illustrates the new GFC control structure with the decoupling controller. It is worth mentioning that the introduced controller works properly with any of the conventional GFC control structures without affecting the steady state operations. It will be tested with the most common GFC control structures, namely, droop control, VSG, and DC-matching control later. It will be proven through the following mathematical steps that the introduced gain improves the decoupling between the two loops and power components. Because of new added decoupling term, (18) is modified to (35),

$$v_{id}^* = k_{i,cd}\emptyset_{i,d} + k_{p,id}\emptyset'_{i,d} \underbrace{-\omega_n L_1 i_{oq}}_{cross-coupling} + K_1 v_{iq}^* \tag{35}$$

State space modelling is derived for the proposed network considering the new equation (35) then linearized as previously mentioned in (34) in a symbolic form. It can be shown from the derived state space matrix that the cross-coupling between $v_{od}$ and $v_{oq}$ ($v_{cross}$) is modified from (36) to (37):

$$v_{cross} = \omega_{pll} \tag{36}$$

$$v_{cross} = \omega_{pll} - k_1 k_{p,cq} k_{p,vq} r_d / L_f \tag{37}$$

Therefore, coupling term depends on the estimated speed $\omega_{pll}$ when $k_1$ is zero and the coupling is reduced as $k_1$ increases. It is worth mentioning that the estimated speed $\omega_{pll}$ during the disturbances in not accurate and the controller takes a while to properly estimate its value. So, the objective of the decoupling block is to reduce the dependency on $\omega_{pll}$. The coupling between the current components is also decreased as shown;

$$i_{cross} = r_d(\omega_{pll} - \omega_n) - k_1 k_{p,cq} r_d / L_f \tag{38}$$

To illustrate the effect of $k_1$ on the coupling graphically, the transfer function between the $v_{id}^*$ and $v_{iq}^*$ is first deduced, then a step change in the $v_{iq}^*$ is applied and the corresponding response on the $v_{id}^*$ is plotted with time. The previous process is performed at different values of $k_1$. Fig. 6 describes the coupling between the direct and quadrature voltage components ($v_{id}^*, v_{iq}^*$) while changing the gain ($k_1$). Coupling between $v_{id}^*$ and $v_{iq}^*$ is significantly reduced during the transients while increasing the value of $k_1$. It is noticed from Fig. 6 that the steady state error for all gains is zero. Therefore, the proposed gain does not affect the steady state responses thanks to the integral action of the PI controller

in the $v_{id}^{*}$ and $v_{iq}^{*}$ that eliminates the steady state error. This efficient decoupling improves the damping characteristics significantly.

*B) Proposed damper controller*

Power oscillations caused by disturbances should be rapidly damped to avoid loss of synchronization between the GFCs. Therefore, the controller structure is modified by an oscillation damping controller to improve the frequency stability. As shown in Fig. 5, The damper is a feedback controller, that provides a stabilizing control signal which is added to the quadrature axis of the injected voltage. This added signal produces an electric torque component that counteracts the frequency deviations. The produced electric damping torque should be in phase with the deviations of the GFCs' frequency to produce a pure damping action. Therefore, the damper controller is mainly constituted by a phase compensation with time constants( $t_1$ and $t_2$). These time constants are designed optimally to supply a phase shift needed to compensate for the phase lag/lead between the voltage and the resulting electric damping torque. Although there are different input signals for the damper controller that can be used to extract the frequency deviations, the active power is used as it is the best indicator for the oscillations, as shown in Fig. 5. The key contribution of the damper is to damp the most sever frequency oscillations to the network stability. Therefore, the participation factor analysis is used to classify the network's oscillations into categories (based on their severity), then according to this classification, the damper controller is designed efficiently. The following section discusses the design process for the proposed hybrid damping method.

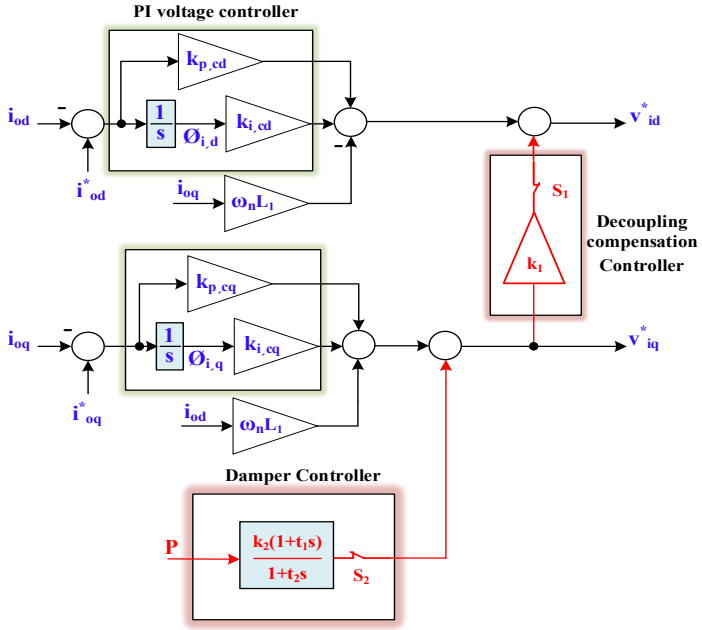


Fig. 5. The proposed hybrid damping method structure introduced for GFC.

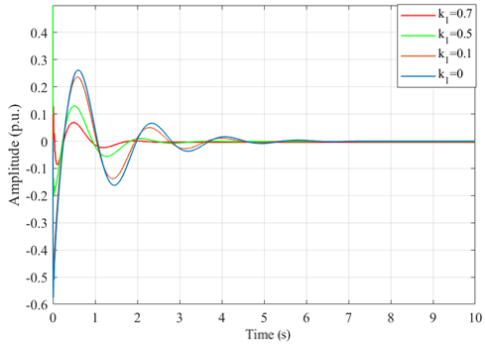


Fig. 6. The coupling between the direct and quadrature control loops.

## 6. THE PROPOSED HYBRID DAMPING METHOD DESIGN.

This section explains how the gain $k_2$ and $t_1, t_2$ for damper controller and the $k_1$ for the decoupling controller are optimally designed to enhance the system performance and improve the damping characteristics.

Oscillations in the power system are classified into three main modes [26], namely, (i) local oscillation mode, which are caused by the LCL filter parameters, the power converter switches, and the connecting line of the power converter to the network, (ii) control oscillation mode, which are caused due to the poor tuning of control parameters, and (iii) interactions oscillation mode (Inter-unit oscillation), which are caused due to the different power sharing between the power converters. These latter oscillations depend on the rating of converter units and the reactance of the distribution lines between the power converters, therefore, the three GFCs in the test network are choose with different rating to include this mode of oscillation, as shown in TABLE 1.

Table 1. System parameters.

| | | |
|---|---|---|
| $\omega_n$ | Nominal network Frequency | $2\pi \times 50$ rad/s |
| $V_n$ | Nominal network Voltage | 320 kV |
| $P_{n1}$, $P_{n2}$ | Nominal power for GFC1, GFC2 | 250 MW |
| $P_{n3}$ | Nominal power for GFC3 | 200 MW |
| $V_{dc1}$, $V_{dc2}$, $V_{dc3}$ | Nominal DC voltage of GFCs (1,2,3) | 640 kV |
| $R_{line}$ | Line resistance | 0.03 Ω/km |
| $L_{line}$ | Line inductance | 0.95 mH/km |
| $C_{line}$ | Line shunt capacitance | 10 nF/km |
| $P_{load1}$, $P_{load2}$, $P_{load3}$ | Power for load 1, load 2, load 3 | 150 MW |

Each mode of oscillation has a specific frequency band. The oscillation frequencies and their damping ratios can be deduced form the eigenvalues of the previously derived state-space matrix. Eigenvalues is described as follows;

$$\lambda_i = \sigma_i \pm j\omega_i \tag{39}$$

where, the real part ($\sigma_i$) relates to damping ratio and the imaginary part ($\omega_i$) is concerned with the frequency of oscillation, as described in the following relation;

$$\zeta = \frac{\sigma}{\sqrt{\sigma^2+\omega^2}} \quad , \quad f = \frac{\omega}{2\pi} \tag{40}$$

There are main challenges for designing the controllers in the interconnected network. First challenge is how to allocate the participation of each GFC or a group of GFCs in each oscillation mode. This challenge is addressed using the concept of participation factors, which discussed in [26] and described as follows;

$$p_{ki} = \frac{|v_{ik}||w_{ki}|}{\sum_{k=1}^{k=n}|v_{ik}||w_{ki}|} \tag{41}$$

where, $v, w$ are known as the right and left eigenvector of matrix A, respectively. $v_{ik}$ relates the $i^{th}$ mode to the $k^{th}$ state variable, that is, the activity of the $i^{th}$ mode in the $k^{th}$ state variable. On the other hand, $w_{ki}$, relates the

weighted contribution of the $k^{th}$ state variable in the $i^{th}$ mode. For instance, considering a mode of oscillation $y$, which is affected by the system states $x_1, x_2, \dots x_i$, then the participation algorithm gives each state a number between 0 and 1 regardless of their unit. As, the number getting closer to 1, the effect of this state in that mode will be maximum. If this state is well controlled, mode of oscillation will be well damped.

Another challenge in power system control is that the wide operating range in interconnected networks. Amount of damping and the oscillation frequency vary with the operating conditions of the power network. The oscillation damping strategy should be designed efficiently considering the whole range of the operating conditions. The main advantages of the proposed method are, (1) the integrated design, as the power converter parameters are designed in the integrative environment considering both the impacts of the other converters and loads, (2) handling a wide range of the operating conditions, (3) considering the multi-vendor interoperability, as the GFCs are controlled by different techniques. Design guidelines for the optimization technique to choose the parameters of the damper and decoupling controller are described in Fig. 7. The flow chart is used in the proposed network through the following steps: (i) First, the algorithm starts by defining different number of operating conditions that commonly appeared in the network in Fig. 1. For simplicity, the design considers 4 conditions, the first condition is the normal operating condition, where GFC-1 operates at 0.62 pu of its nominal power with PLL and droop technique, GFC-2 operates at 0.62 pu with VSG technique and GFC-3 operates at 0.62 pu with DC-matching technique. The GFCs are set to operate at 0.62 pu to cover the third operating condition which compensate for any converter failure and allow the other two converters to supply the load. The second condition includes a step change in load as the power withdrawn from load 3 is doubled. The third case occurs when the distribution line connecting between Bus 4 and Bus 9 is disconnected. The fourth condition includes the outage of the GFC-2. (ii) For every network condition, the non-linear models are constructed based on the derived equations in section III. (iii) Derived non-linear models are linearized using equation (34) and the corresponding linear state spaces models are derived. (iv) Each state space model from the 4 linearized models, the natural responses $\omega_n^i$, $\zeta^i$ damping ratio vectors and the participation factor matrix $M_{pf}^i$ are determined where $i$ is an iteration over the linearized models. (v) After that the oscillations are classified into bands according to their severity, effect, and contribution on the responses. For instance, the algorithm defines 3 bands that target the oscillations in the power components, which are; (1) $\mathrm{M}^1$ is a band that contains the mode of oscillations within $0 < \omega_n^i \leq 50$ and has a damping ratio $\zeta^i < 100\%$ and participation factor ($pf_P{}^i$ *or* $pf_Q{}^i$) > 0.5. (2) $\mathrm{M}^2$ is a band that contains the mode of oscillations within $50 < \omega_n^i < \infty$ and has a damping ratio $\zeta^i < 100\%$ and ($pf_P{}^i$ *or* $pf_Q{}^i$) > 0.5. (3) $\mathrm{M}^3$ is a band that contains the mode of oscillations within $0 < \omega_n^i < \infty$ and has a damping ratio $\zeta^i < 100\%$ and ($pf_P{}^i$ *or* $pf_Q{}^i$) < 0.5. (vi) Construct the objective function, for simplicity, the objective function is designed to handle the oscillations in the active and reactive power responses. However, it can be extended to handle more states. The constructed objective function gives a weighting factor for each band from the 3 bands. These weighting factors are determined according to how the oscillations in their band will deteriorate the active and reactive power responses. The pattern search is used to maximize the damping ratios according to the participation and weighting factors as shown in the following objective function:

$$\max \sum_{i=1}^{o} \left[ w_1 \left[ \zeta_1^i \times \boldsymbol{pf_{1P}}^i \right] + w_2 \left[ \zeta_2^i \times \boldsymbol{pf_{2P}}^i \right] + w_3 \left[ \zeta_3^i \times \boldsymbol{pf_{3P}}^i \right] \right] + \left[ w_1 \left[ \zeta_1^i \times \boldsymbol{pf_{1Q}}^i \right] + w_2 \left[ \zeta_2^i \times \boldsymbol{pf_{2Q}}^i \right] + w_3 \left[ \zeta_3^i \times \boldsymbol{pf_{3Q}}^i \right] \right]$$

where, $\boldsymbol{pf_{1P}}^i$, $\boldsymbol{pf_{2P}}^i$ and $\boldsymbol{pf_{3P}}^i$ are the participation vector of the active power related to the operating point $i$ in the sets $\mathrm{M}^1$,$\mathrm{M}^2$ and $\mathrm{M}^3$, respectively. $w_1$, $w_2$ and $w_3$ are weighting factors for the sets $\mathrm{M}^1$ ,$\mathrm{M}^2$and $\mathrm{M}^3$, respectively. These weightings have values of 0.5, 0.3, 0.2 in the program. $\boldsymbol{\zeta_1^i}$,$\boldsymbol{\zeta_2^i}$ and $\boldsymbol{\zeta_3^i}$ are the damping ratio vectors related to the operating point $i$ in the sets $\mathrm{M}^1$,$\mathrm{M}^2$and $\mathrm{M}^3$respectively. $\boldsymbol{pf_{1Q}}^i$, $\boldsymbol{pf_{2Q}}^i$ and $\boldsymbol{pf_{3Q}}^i$ are the participation vector of the reactive power.

| P1 | Q1 | $\zeta$ | $\omega_n$ |
|---|---|---|---|
| Before the optimization | | | |
| 1 | 1 | 100% | 50.2 |
| 1 | 1 | 100% | 50.2 |
| 0.9 | 1 | 91% | 50.2 |
| 0.9 | 1 | 91% | 50.2 |
| 0.4 | 0 | 19% | 3.7 |
| 0.4 | 0 | 19% | 3.7 |

| P1 | Q1 | $\zeta$ | $\omega_n$ |
|---|---|---|---|
| After the optimization | | | |
| 0.2 | 0 | 100% | 331.6 |
| 0.1 | 0 | 100% | 153.8 |
| 0.7 | 0 | 100% | 45.3 |
| 0 | 0.8 | 100% | 50.2 |
| 0 | 1 | 100% | 50.2 |
| 0.6 | 0.1 | 99% | 22.3 |

Table 2. Active and reactive power responses characteristics

| | | | |
|---|---|---|---|
| 0.6 | 0.1 | 99% | 22.3 |
| 0.1 | 0 | 98% | 9.2 |
| 0.1 | 0 | 98% | 9.2 |

(vii) Finally, the control parameters are modified based on pattern search optimization technique to maximize the previous objective function. Then, keep repeating the whole process if the stopping criteria is not satisfied. The state space model for the overall system given in Fig. 1 consists of 54 states. Therefore, it will be difficult to illustrate the whole results. So, the results related to power converter 1 active and reactive power components are only illustrated in Table 2. It is worth mentioning that the efficient damping characteristics in the converter powers will be reflected on the converter voltage and current due to their relationship. As shown in Table 2 (before the optimization), although, the oscillation of natural frequency that equals to 50.26 has a highly participation factor on the active and reactive power components, its damping ratio is 100%. The oscillation of natural frequency equal to 50.28 has a high participation factor on the active and reactive powers and its damping ratio is slightly small and equal to 91%. Therefore, this type of oscillation deteriorates the power responses. Finally, the oscillation with natural frequency equal to 3.77 have a small participation factor on the active power, but its damping ratio is inefficient. Therefore, the oscillation of 3.77 will significantly deteriorates the active power response. The frequency band near to the 50.283 gives a good intuition about the coupling between the active and reactive power as it has a maximum participation factor in the active and reactive powers simultaneously. The problem of the coupling and damping have been addressed using the proposed hybrid damping method, as shown Table 1 (after the optimization), there is no coupling between the active and reactive power components over all the frequency bands that deteriorate the power responses except at the oscillation with natural frequency that equals to 22.35 Hz, however, with a small sharing participation factor near to zero. Hence, the coupling is significantly reduced. Damping characteristics of the power is significantly improved as the damping ratio for all the frequency bands are above the 98% and with small participation factors.

## 7. CONTROL HARDWARE IN THE LOOP VALIDATION

The proposed method is practically validated through control hardware in the loop (CHiL) using OPAL-RT, as shown in Fig. 8. The model for every GFC comprises two main parts. The first part is the plant model, which includes the power converter, PWM module, LCL filter and dc-link. The second part is the controller model that

consists of the transformation between frames and main control loops. For simplicity, the controller model for power converter 1 is uploaded on a DSP labelled as TMS320F28335ZJZA. The remaining model (transmission lines, buses, loads, other two GFCs models and the plant model for power converter 1) will be implemented on the OPAL-RT. The DSP is responsible for handling the control and feedback signals from the plant model of power converter 1 and another network parts setup on OPAL-RT platform. The DSP receives GFC 1 output currents and the voltage across the LCL filter and based on these values it generates the required signals to operate the GFC 1 on OPAL-RT platform. The improved controllers for the GFCs have been tested against many common disturbances in the power grid, which could be described as follows; As shown in period A into the Figures 9-12: a three phase to ground non-permanent fault occurs at Bus 3 during t =1.5 s. In period B: the fault is cleared (post-fault condition) at t=1.65 s. This paper only addresses the damping issues at the fault and post-fault instances but checking the existence of an equilibrium point after the fault

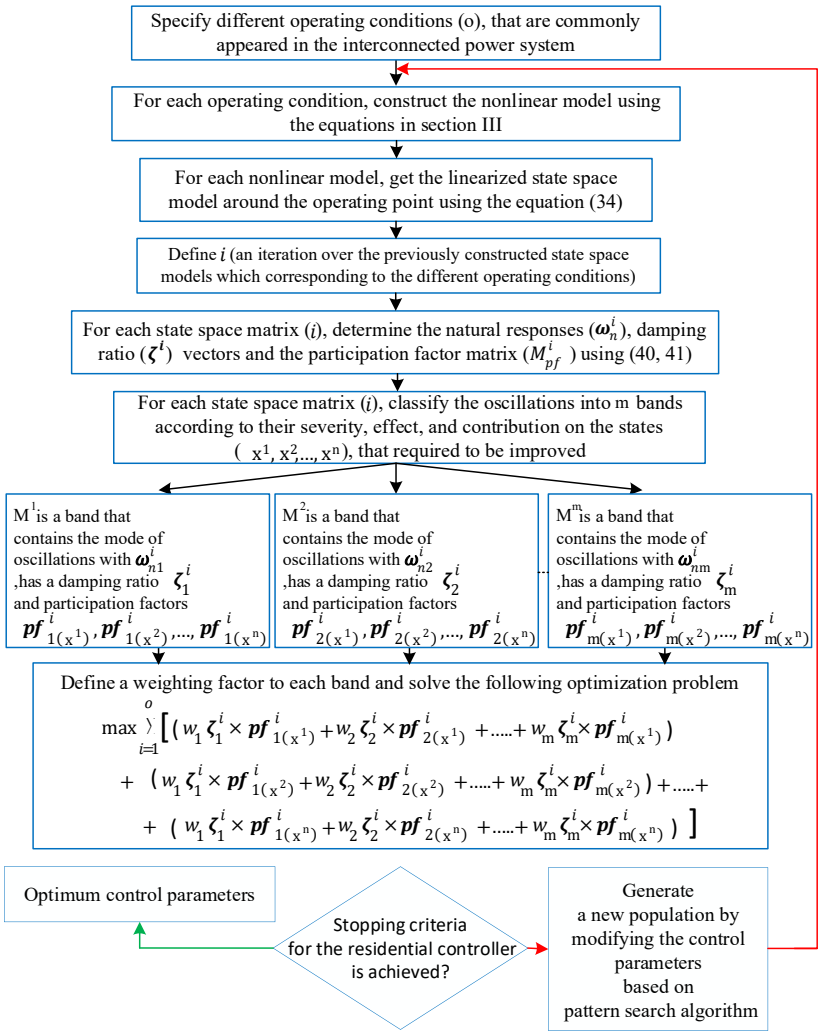


Fig. 7. The Flow chart for designing the GFC's controller parameters.

conditions is out of the paper scope. In period C: a loss of transmission line connected between Bus 5 and Bus 9 at t =3.5 s. In period D: recovery of transmission line connected between Bus 5 and Bus 9 takes place at t = 4.5 s. In period E: a step change in load 2 takes place from 150 MW to 300 MW at t = 5.5 s. In period F: a step change in load 2 takes place from 300 MW to 150 MW at t =6.5 s. In period G: loss of GFC 3 and the transmission lines are connected between Bus5, Bus4 and Bus 9 at t = 8 s. In order to investigate the interoperability under different control methods, each GFC is controlled by a different control method, namely, GFC-1 operates with PLL and droop technique [27] while GFC-2 and GFC-3 use VSG [28] and DC-matching technique [21], respectively. To verify the effectiveness of the additional hybrid damping method on the dynamic performance, two case studies are tested. The first case study will investigate responses of the three converters alone without adding the hybrid method (undamped case), whereas the other case study investigates the responses where the proposed hybrid method is adapted to each converter's technique (damped case). Fig. 9 illustrates the output active power of the three GFCs against the previously stated large disturbances. Fig.

9(a) depicts the output active power of GFC-1 with and without the additional hybrid damping method. In the period A where a three phase to ground fault occurs at Bus 3, the active powers in the undamped case suddenly drops near to zero, and the response has an insufficient damping with maximum overshoot of 0.6 pu with oscillations peak of 0.1 pu till the fault is cleared at the beginning of period B. However, as shown in Fig. 9(a) with the additional hybrid damping, the power oscillation during this period is properly damped with a maximum overshoot of 0.05 pu. During the postfault period, the responses provide the same settling time of 0.45 s but with improper damped oscillations in the undamped case, as shown in period B in Fig 9(a). Moreover, the oscillations are scoped and well damped by the optimization algorithm, as shown in Fig 9(a) with the proposed hybrid damping method compared to the undamped case. During the loss and the reconnection of a transmission line in periods C and D, respectively, the active power sharing among the GFC does not change, however, the settling time and the damping characteristics are significantly improved with the additional damping (0.6 s with max overshoot of 0.25 pu in the undamped case and 0.4 s with maximum overshoot of 0.14 pu in the damped case). As shown in Fig. 9(a) period E and F, the proposed hybrid damping method provides an efficient characteristic during step load change (0.3 s with max overshoot of 0.27 pu in the undamped case and 0.1 s with maximum overshoot of 0.25 pu in the damped case). Furthermore, the additional hybrid damping method also provides an efficient characteristic during the outage of GFC 3, as the active power will be zero for this converter and the remaining converters will smoothly modify their output powers (to compensate the loss of converter 3) with damped oscillations as shown in Fig 9(a) period G against the undamped case. Fig 9(b) and Fig. 9 (c) depict the output active powers of GFC-2 and GFC-2, respectively. With the additional damping method, oscillations are properly damped for all studied periods, resulting in superior transient performance compared to the undamped case. As demonstrated in Fig. 9 the extra damping appropriately works with different control methods, which reflects the adaptability of the proposed hybrid damping approach to each of those control techniques

Table 3 proves the superior damping characteristics of the proposed hybrid damping method against the undamped case. The Table includes the damping characteristics in terms of maximum overshoot and settling time for the worst GFC' active power response. It can be confirmed that the maximum overshoot and settling time are reduced by 0.25 pu and 0.5 s on average, respectively.

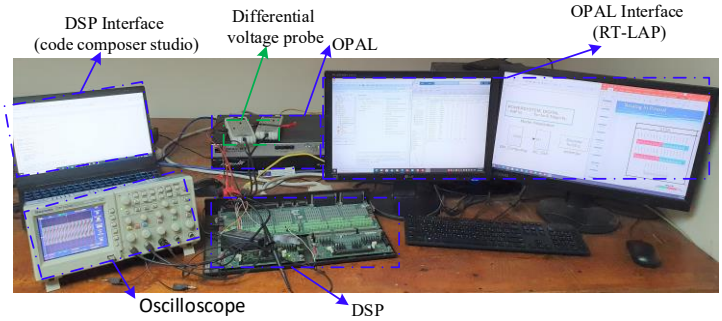


Fig. 8. Control-hardware-in-the-loop test rig.

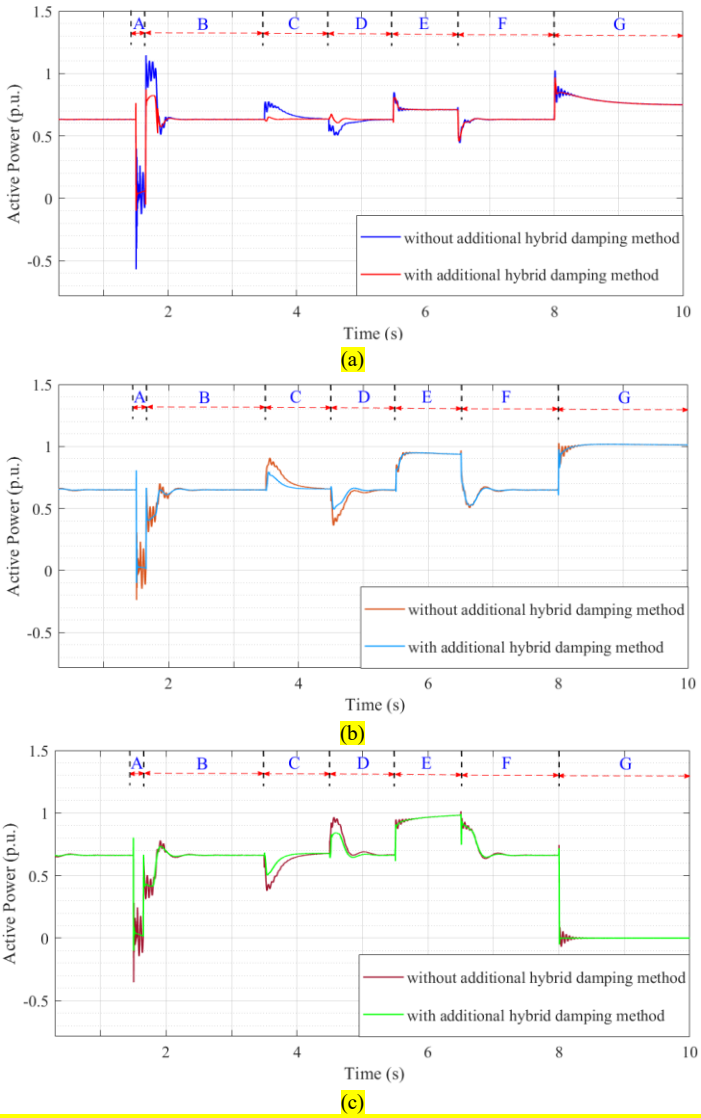


Fig. 9. Experimental results for GFCs' active powers with/without the additional hybrid damping method: (a) active power response for GFC1 (controlled by PLL technique), (b) active power response for GFC2 (controlled by VSG technique), and (c) active power response for GFC3 (controlled by DC matching technique).

Table 3. The oscillation damping characteristics of the proposed and conventional damping methods.

| | Without the proposed hybrid damping method | | With the proposed hybrid damping method | |
|---|---|---|---|---|
| | Maximum overshoot (pu) | Settling time (s) | Maximum overshoot (pu) | Settling time (s) |
| Period A | 0.60 | > 0.15 | 0.05 | 0.05 |
| Period B | 0.34 | 0.6 | 0.10 | 0.1 |
| Period C | 0.28 | 1.0 | 0.13 | 0.13 |
| Period D | 0.30 | 1.2 | 0.14 | 0.14 |
| Period E | 0.16 | 0.3 | 0.07 | 0.07 |
| Period F | 0.44 | 0.7 | 0.15 | 0.15 |
| Period G | 0.27 | 1.0 | 0.14 | 0.14 |

Fig. 10 illustrates the output reactive power for the three GFCs against the previously stated large disturbances. Fig. 10(a), Fig. 10(b), and Fig. 10(c) compares between the undamped case and damped case for the GFC-1, and GFC-2 and GFC-3, respectively. Over all disturbances, the additional proposed hybrid method provides an efficient damping and decoupling against the undamped case. Therefore, the oscillations in active power will not be translated to the reactive power and vice versa.

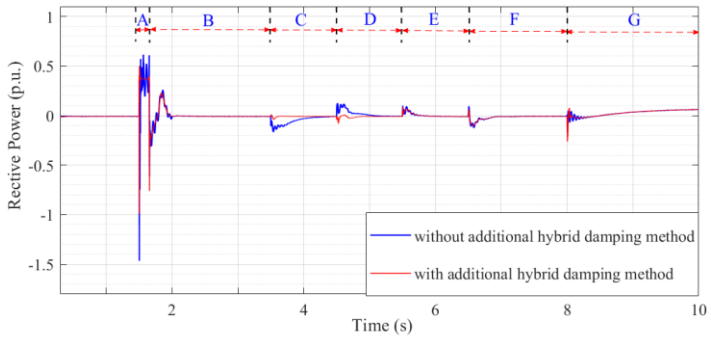


(a)

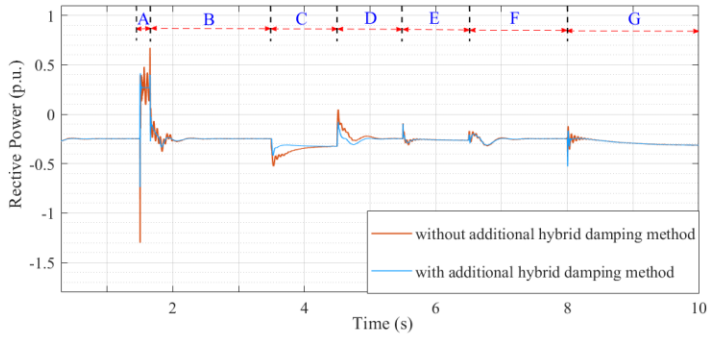


(b)

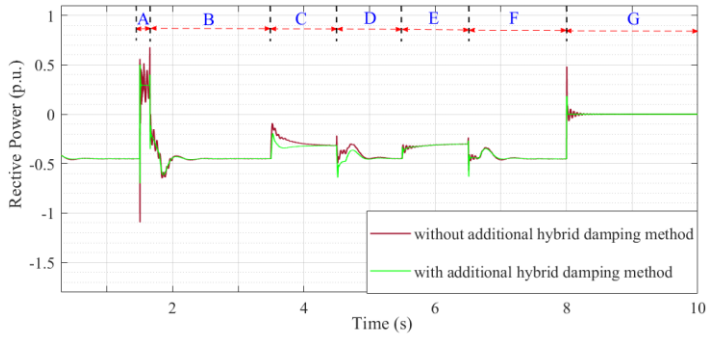


(c)

Fig. 10. Experimental results for GFCs' reactive powers with/without the additional hybrid damping method: (a) reactive power response for GFC1 (controlled by PLL technique), (b) reactive power response for GFC2 (controlled by VSG technique), and (c) reactive power response for GFC3 (controlled by DC matching technique).

Fig. 11 illustrates the output voltage for the three GFCs against the previously stated large disturbances. Fig. 11(a), Fig. 11(b), and Fig. 11(c) compares the voltage response between the undamped case and damped case for the GFC-1, and GFC-2 and GFC-3, respectively. It is clearly illustrated that the additional hybrid damping provides voltage responses with damped oscillations. It is worth mentioning that the optimization technique focuses on improving the damping characteristics for the active and reactive power components, and hence, the voltage responses are also improved accordingly. Fig. 12 illustrates the frequency for the three GFCs against the previously stated large disturbances. Fig. 12(a), Fig. 12(b), and Fig. 12(c) compares the output frequency response between the undamped case and damped case for the GFC-1, and GFC-2 and GFC-3, respectively. It is clearly illustrated that controlling the GFCs with the proposed hybrid damping method will provide a fast synchronization between the GFCs against all the disturbances. For instance, during the loss of the transmission line at 3.5 s (period C), the GFCs with the proposed method will be synchronized within 0.3 s against 1 s with the undamped case. Moreover, the droop characteristic is clearly appeared in the frequency response, as in the heavily loading condition, where the frequency slightly drops below the nominal value. During light loading condition, the frequency will be above the nominal value. This droop characteristic is very important in the power system network as it gives a good intuition about the loading condition without a communication link among the GFCs.

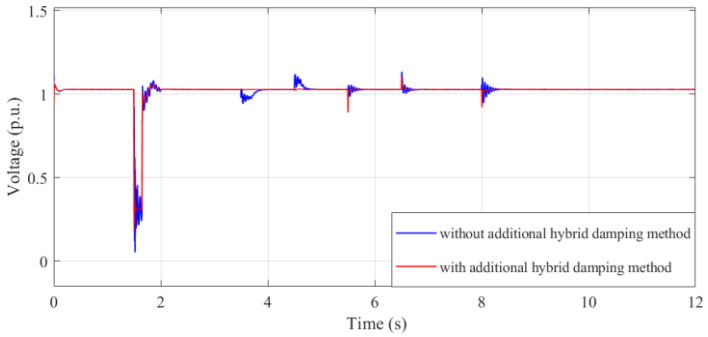


(a)

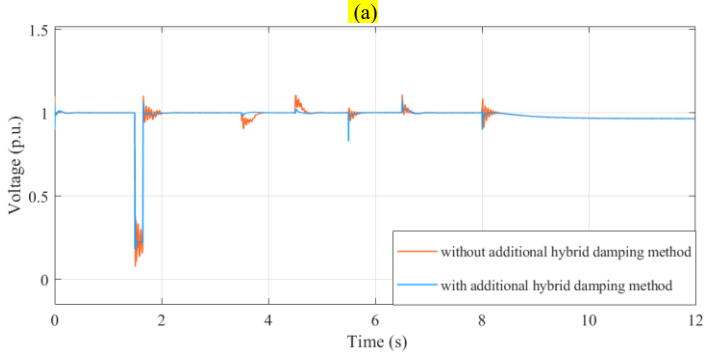


(b)

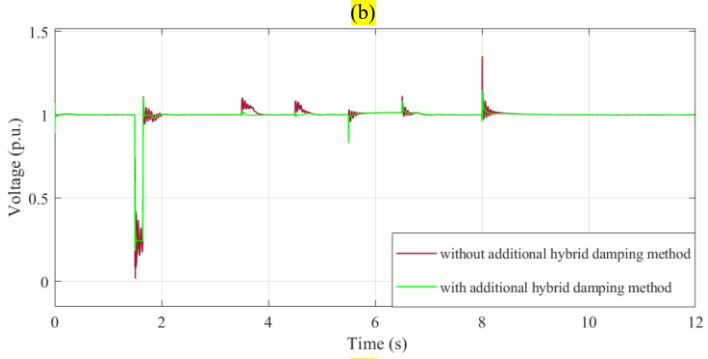


(c)

Fig. 11. Experimental results for GFCs' output voltages with/without the additional hybrid damping method: (a) voltage response for GFC1 (controlled by PLL technique), (b) voltage response for GFC2 (controlled by VSG technique), and (c) voltage response for GFC3 (controlled by DC matching technique).

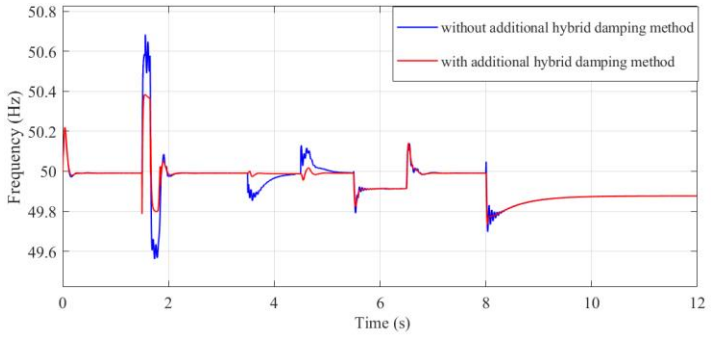


(a)

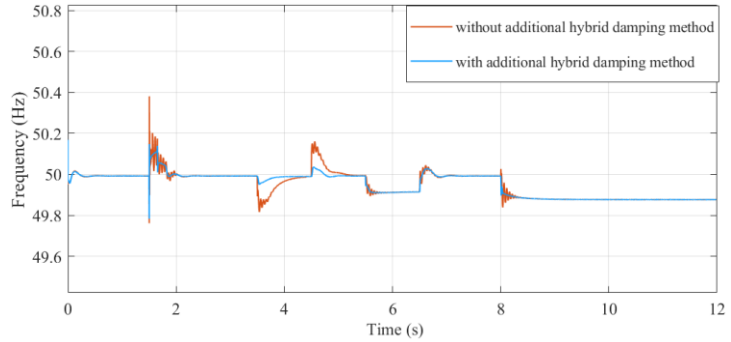


(b)

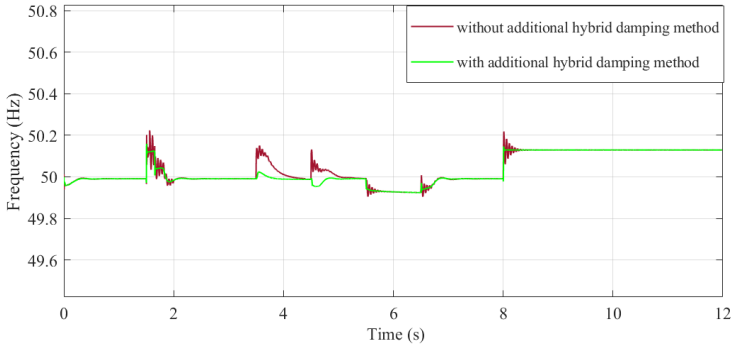


(c)

Fig. 12. Experimental results for GFCs' output frequencies with/without the additional hybrid damping method: (a) frequency response for GFC1 (controlled by PLL technique), (b) frequency response for GFC2 (controlled by VSG technique), and (c) frequency response for GFC3 (controlled by DC matching technique).

## 8. ACKNOWLEDGEMENT

This work was supported by the Deputyship for Research and Innovation, the Ministry of Education in Saudi Arabia, project number (1071).

## 9. CONCLUSION

This paper proposed a new hybrid damping method to efficiently damp the whole interconnected GFCs-based power network oscillations. The proposed method operates efficiently in the interconnected GFCs-based power network including the interoperability under different control methods. Parameters for the proposed damping method have been optimally designed using pattern search and participation factor analysis. Optimum control parameter selection has been taken into consideration the possibility of many operating conditions. The proposed damping method has been validated using Control Hardware in the Loop (CHiL) against common types of network disturbances, namely, the fault conditions, loss of transmission line/GFC and step change in the loads. Moreover, the problem of multi reference has been considered in the study. The results reflected better and faster damping for the proposed hybrid damping method against conventional damping techniques. Overall, the maximum overshoot and settling time are reduced by 0.25 pu and 0.5 s on average, respectively, using the proposed hybrid method.

## References

[1] X. Xiong, C. Wu, B. Hu, D. Pan, and F. Blaabjerg, "Transient Damping Method for Improving the Synchronization Stability of Virtual Synchronous Generators," *IEEE Transactions on Power Electronics,* 2020.

[2] Y. Deng, Y. Tao, G. Chen, G. Li, and X. He, "Enhanced power flow control for grid-connected droop-controlled inverters with improved stability," *IEEE Transactions on Industrial Electronics,* vol. 64, no. 7, pp. 5919-5929, 2016.

[3] W. Du *et al.*, "A comparative study of two widely used grid-forming droop controls on microgrid small-signal stability," *IEEE Journal of Emerging Selected Topics in Power Electronics,* vol. 8, no. 2, pp. 963-975, 2019.

[4] M. Ebrahimi, S. A. Khajehoddin, and M. Karimi-Ghartemani, "An improved damping method for virtual synchronous machines,"

*IEEE Transactions on Sustainable Energy,* vol. 10, no. 3, pp. 1491-1500, 2019.
[5] D. Carletti, A. Eduardo Alves Amorim, T. Silva Amorim, D. Sávio Lyrio Simonetti, J. Farias Fardin, and L. Frizera Encarnacao, "Adaptive Armature Resistance Control of Virtual Synchronous Generators to Improve Power System Transient Stability," *Energies 2020,* vol. 13, no. 9, p. 2365, 2020.
[6] J. R. Pérez, J. A. Suul, S. D'Arco, A. Rodríguez-Cabero, and M. Prodanovic, "Virtual synchronous machine control of VSC HVDC for power system oscillation damping," in *IECON 2018-44th Annual Conference of the IEEE Industrial Electronics Society*, 2018, pp. 6026-6031: IEEE.
[7] C. Arghir, T. Jouini, and F. Dörfler, "Grid-forming control for power converters based on matching of synchronous machines," *Automatica,* vol. 95, pp. 273-282, 2018.
[8] P. Unruh, M. Nuschke, P. Strauß, and F. Welck, "Overview on grid-forming inverter control methods," *Energies 2020,* vol. 13, no. 10, p. 2589, 2020.
[9] R. Yin, Y. Sun, S. Wang, and L. Zhang, "Stability Analysis of the Grid tied VSC Considering the Influence of Short Circuit Ratio and X/R," *IEEE Transactions on Circuits Systems II: Express Briefs,* 2021.
[10] J. Z. Zhou, H. Ding, S. Fan, Y. Zhang, and A. M. Gole, "Impact of Short-Circuit Ratio and Phase-Locked-Loop Parameters on the Small-Signal Behavior of a VSC-HVDC Converter," *IEEE Transactions on Power Delivery,* 2014.
[11] S. Laudahn, J. Seidel, B. Engel, T. Bülo, and D. Premm, "Substitution of synchronous generator based instantaneous frequency control utilizing inverter-coupled DER," in *2016 IEEE 7th International Symposium on Power Electronics for Distributed Generation Systems (PEDG)*, 2016, pp. 1-8: IEEE.
[12] S. Dong and Y. C. Chen, "Adjusting synchronverter dynamic response speed via damping correction loop," *IEEE Transactions on Energy Conversion,* vol. 32, no. 2, pp. 608-619, 2016.
[13] Y. Chen, R. Hesse, D. Turschner, and H.-P. Beck, "Improving the grid power quality using virtual synchronous machines," in *2011 International Conference on Power Engineering, Energy and Electrical Drives*, 2011, pp. 1-6: IEEE.
[14] L. Yang *et al.*, "Effect of phase-locked loop on small-signal perturbation modelling and stability analysis for three-phase LCL-type inverter connected to weak grid," *IET Renewable Power Generation,* vol. 13, no. 1, pp. 86-93, 2019.
[15] M. Ebrahimi, S. A. Khajehoddin, and M. Karimi-Ghartemani, "An improved damping method for virtual synchronous machines," *IEEE Transactions on Sustainable Energy,* vol. 10, no. 3, pp. 1491-1500, 2019.
[16] S. Dong and Y. C. Chen, "Reducing Transient Active-and Reactive-power Coupling in Virtual Synchronous Generators," in *2019 IEEE 28th International Symposium on Industrial Electronics (ISIE)*, 2019, pp. 1090-1095: IEEE.
[17] M. Rasheduzzaman, J. A. Mueller, and J. W. Kimball, "An accurate small-signal model of inverter-dominated islanded microgrids using $ dq $ reference frame," *IEEE Journal of Emerging Selected Topics in Power Electronics,* vol. 2, no. 4, pp. 1070-1080, 2014.
[18] Y. Li, R. Qi, and S. Wang, "New control schemes of output power decoupling based on synchronverter," in *2018 21st International Conference on Electrical Machines and Systems (ICEMS)*, 2018, pp. 1980-1985: IEEE.
[19] P. Zhang, H. Zhao, H. Cai, J. Shi, and X. He, "Power decoupling strategy based on 'virtual negative resistor'for inverters in low-voltage microgrids," *IET Power Electronics,* vol. 9, no. 5, pp. 1037-1044, 2016.
[20] Z. A. Obaid, L. Cipcigan, M. T. J. R. Muhssin, and S. E. Reviews, "Power system oscillations and control: Classifications and PSSs' design methods: A review," vol. 79, pp. 839-849, 2017.
[21] L. Huang *et al.*, "A virtual synchronous control for voltage-source converters utilizing dynamics of DC-link capacitor to realize self-synchronization," *IEEE Journal of Emerging Selected Topics in Power Electronics,* vol. 5, no. 4, pp. 1565-1577, 2017.
[22] T. Messo, A. Aapro, T. Suntio, and T. Roinila, "Design of grid-voltage feedforward to increase impedance of grid-connected three-phase inverters with LCL-filter," in *2016 IEEE 8th International Power Electronics and Motion Control Conference (IPEMC-ECCE Asia)*, 2016, pp. 2675-2682: IEEE.
[23] R. Henriquez-Auba, J. D. Lara, C. Roberts, and D. S. Callaway, "Grid forming inverter small signal stability: Examining role of line and voltage dynamics," in *IECON 2020 The 46th Annual Conference of the IEEE Industrial Electronics Society*, 2020, pp. 4063-4068: IEEE.
[24] X. Wang, Y. W. Li, F. Blaabjerg, and P. C. Loh, "Virtual-impedance-based control for voltage-source and current-source converters," *IEEE Transactions on Power Electronics,* vol. 30, no. 12, pp. 7019-7037, 2014.
[25] J.-O. Baek and S. Kim, "Detection and Analysis of Electromechanical Oscillation in Power Systems with Low-Sampled Data Using Modal Analysis Methods," *Journal of Electrical Engineering & Technology,* vol. 15, no. 5, pp. 1999-2006, 2020/09/01 2020.
[26] B. Pal and B. Chaudhuri, *Robust control in power systems*. Springer Science & Business Media, 2006.
[27] E. Rokrok, T. Qoria, A. Bruyere, B. Francois, and X. Guillaud, "Classification and dynamic assessment of droop-based grid-forming control schemes: Application in HVDC systems," *Electric Power Systems Research,* vol. 189, p. 106765, 2020.
[28] S. D'Arco, J. A. Suul, and O. B. Fosso, "A Virtual Synchronous Machine implementation for distributed control of power converters in SmartGrids," *Electric Power Systems Research,* vol. 122, pp. 180-197, 2015.